

# Research on Aerodynamic Characteristics of Hovering Rotor Based on Leading Edge Droop

LI Congcong<sup>1,2</sup>, SHI Yongjie<sup>2\*</sup>, XU Guohua<sup>2</sup>, MA Taihang<sup>2</sup>

1. Shanghai Aircraft Design and Research Institute, Shanghai 201210, P.R.China;

2. National Key Laboratory of Science and Technology on Rotorcraft Aerodynamics, Nanjing University of Aeronautics and Astronautics, Nanjing 210016, P.R.China

(Received 25 April 2021; revised 10 June 2021; accepted 15 July 2021)

**Abstract:** In view of the reduction of hovering efficiency near high tension when a helicopter rotor hovers, a numerical simulation method of lifting rotor hovering aerodynamic characteristics based on leading edge droop is established in this paper. It is dominated by Reynolds average N-S equation in integral form. Firstly, VR-12 airfoil is taken as the research object, and the influence of leading edge droop angle on the aerodynamic characteristics of two-dimensional airfoil is studied. Secondly, the modified 7A rotor is taken as the research object, and the effects of different leading edge droop angles at the position of blade  $r/R=0.75-1$  on the aerodynamic characteristics in hover are explored. It is found that the leading edge droop can significantly improve the aerodynamic characteristics of two-dimensional airfoil and three-dimensional hovering rotor near high angle of attack, and can effectively inhibit the generation of stall vortex.

**Key words:** helicopter rotor; hovering; leading edge droop; aerodynamic characteristics

**CLC number:** V211.52

**Document code:** A

**Article ID:** 1005-1120(2021)S-0010-07

## 0 Introduction

When a helicopter is the hovering state, with the increase of the collective pitch angle  $\theta_0$ , the lift coefficient and the torque coefficient increase, and the figure of merit  $F_M$  of the helicopter rises to the highest point and then decreases. The figure of merit of the rotor decreases when it is pulled in large force, which affects the flight performance of the helicopter rotor. A series of studies on aerodynamic characteristics of helicopter rotor have been carried out world-wide. Refs.[1-2] used numerical simulation methods and test methods to study the influence of leading edge dynamic droop on the dynamic stall of two-dimensional airfoil. After a series of parametric studies, the optimal control parameters were obtained. In Ref.[3], a rotor with extendable chord length was used to study its influence on the flight envelope and performance of the helicopter.

Some scholars have also carried out a series of numerical simulation studies on active flow control methods of the aerodynamic characteristics of the elevated rotor airfoil<sup>[4-6]</sup>. In addition, Refs.[7-11] studied the influence of blade geometry, like blade tip sweep, on the hover performance of the improved rotor. Ref.[12] studied the effects of tip slots on the aerodynamic characteristics of helicopter rotors using unstructured overset grids. Numerical results show that tip slots can improve the lift coefficient of the airfoil at the tip of the rotor blade and reduce the strength of the rotor blade tip vortex. In Ref.[13], a genetic algorithm is adopted to optimize the blade profile design of the advancing side of disk, so as to achieve the improved aerodynamic characteristics of the rotor. In this paper, combined with the moving overset mesh and the radial basis function(RBF) mesh deformation method, the leading edge droop method is used to study its influence

\*Corresponding author, E-mail address: shiyongjie@nuaa.edu.cn.

**How to cite this article:** LI Congcong, SHI Yongjie, XU Guohua, et al. Research on aerodynamic characteristics of hovering rotor based on leading edge droop[J]. Transactions of Nanjing University of Aeronautics and Astronautics, 2021, 38(S):10-16.

<http://dx.doi.org/10.16356/j.1005-1120.2021.S.002>

on the aerodynamic characteristics of the elevated two-dimensional airfoil and the three-dimensional hovering rotor.

## 1 Numerical Methodology

### 1.1 Governing equations of flowfield

In order to capture the vortex flow characteristics of unsteady flow field, compressible N-S equation is adopted as the governing equation of flow field solution

$$\frac{\partial}{\partial t} \iiint_{\Omega} \mathbf{W} d\Omega + \iint_{\partial\Omega} (F_c - F_v) dS = 0 \quad (1)$$

where  $\mathbf{W}$  is the conservation variable.  $\Omega$  and  $S$  are the volume and surface of the control body respectively, and  $F_c$  and  $F_v$  the flux to the flow and viscosity, respectively. The Roe flux differential splitting scheme is used for spatial dispersion, the implicit LU-SGS method is used for time propulsion, and the turbulence model is SST  $k-\omega$ .

### 1.2 Overset mesh and mesh deformation technique

The motion overset mesh system used in this paper consists of a background grid and a fitting grid around the rotor. In this method, holes are dug in the corresponding area of the background grid through hole unit identification and contribution unit search at the overlapping interface between the blade grid area and the background grid, as shown in Fig.1. During the rotation of the blade grid around the axis, the overlapping area is updated with the movement of the blade grid. In order to realize the information transmission between the blade grid area and the background grid, the distance weighting method is used to interpolate the adjacent grid cells.

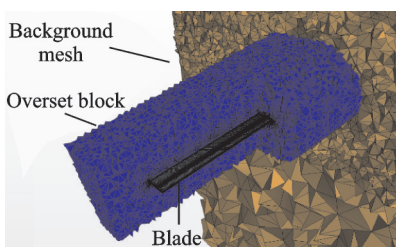


Fig.1 Overset mesh diagram

The mesh deformation method is used to realize the deformation of specified leading edge drooping. Deformation uses the control point displacement to generate an interpolation field for the region and then uses the interpolation field to shift the grid node to the new position. The mesh nodes are redistributed according to the boundary displacements so that the mesh can be non-rigid. The grid deformation uses RBF interpolation method, and the control point  $i$  and its designated displacement  $d'_i$  are used to create the equation, in which the known displacement of each control node is expanded as

$$d'_i = \sum_{j=1}^N f_{b,j}(r_{ij}) \lambda_j + a \quad (2)$$

where  $f_{b,j}(r_{ij})$  is the radial basic function of the shape,  $r_{ij}$  the distance amplitude between two nodes,  $\lambda_j$  the expansion coefficient, and  $N$  the number of control nodes. Fig.2 is the schematic diagram of grid deformation after  $0.75R-R$  part droop angle  $\delta_m = 10^\circ$ . The red part is the rigid pendulous part of the leading edge. In order to prevent the sharp angle and other mesh deformation occurring when the main blade part is connected with the leading edge droop part, the blue part is set as linear floating deformation for smooth connection between the two parts.

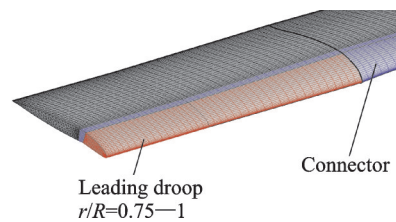


Fig.2 Blade pattern with leading edge droop

### 1.3 Validation

In order to verify the validity of the calculation method in this paper, an example is given to verify the hovering state of the 7A rotor with the existing test data. The rotor is equipped with four rectangular blades, configured by OA209 and OA213 airfoil sections, with piecewise linear negative torsion. Rotor radius  $R$  is 2.1 m and chord length is 0.14 m. The comparison of pressure coefficient  $C_p$  with

$r/R=0.825$  and  $0.975$  is shown in Fig. 3. It can be seen that the calculated  $C_p$  of the rotor surface in this paper is in good agreement with the test value<sup>[14]</sup>. The results show that the proposed method can simulate the hover state of the rotor effectively.

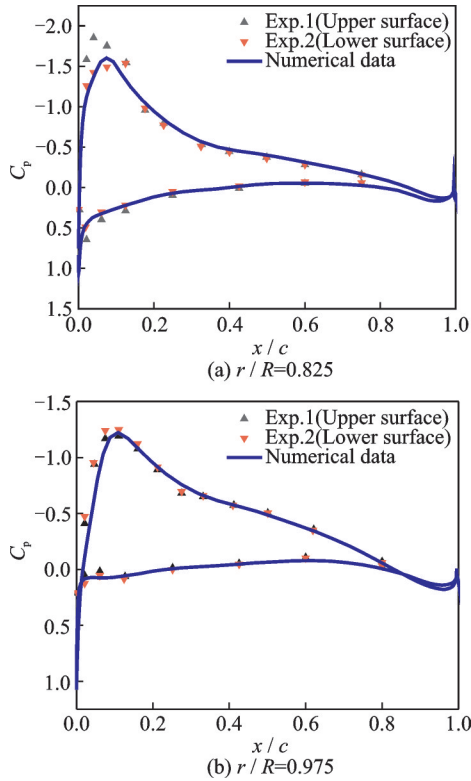


Fig.3 Comparison of experimental and computed results of pressure coefficient  $C_p$

## 2 Influence of Leading Edge Droop on Aerodynamic Characteristics of Airfoils

Firstly, the influence of the fixed droop angle of the leading edge on the aerodynamic characteristics of 2-D airfoils is studied. In this paper, VR-12 airfoil is selected, chord length  $c$  is 0.35 m, inlet Mach number is 0.45, and the fixed drooping part of the leading edge of airfoil is  $c/4$  from the leading edge. In order to prevent the connection between the drooping part of the leading edge and the fixed part of the trailing edge from appearing too sharp bending angle during the mesh deformation process, the width of  $2\%c$  at the middle connection is set as linear connection, which is more in line with the ac-

tual situation.

The states of  $5^\circ$ ,  $8^\circ$  and  $10^\circ$  of the leading droop angle are calculated and the aerodynamic characteristics of airfoils under different droop angles are compared with the reference state, as shown in Fig. 4. It can be seen that the stall angle of attack of the airfoil is significantly increases when the leading edge droop is used, and the drag coefficient at  $16^\circ$  angle of attack is also significantly reduced. After the leading edge of the airfoil droops, the entire airfoil changes from the lifting moment to the lowering moment relative to the datum state. When the angle of attack is small, the lift coefficient  $C_l$  decreases slightly with the increase of the droop angle of the leading edge. This is because after the leading edge droops, the relative angle of attack of the leading edge decreases, so the lift force of this part decreases. The increase of leading edge droop angle has no obvious effect on lift coefficient  $C_l$  and drag coefficient  $C_d$ . The bow moment  $C_m$  caused by too large droop angle at small angle of attack may have negative effects on flight control and blade vibration.

Fig.5 shows a comparison of the airfoil surface flow diagram near the high angle of attack. When  $\alpha = 14^\circ$  and  $16^\circ$ , stall vortexes of a certain size exist near the trailing edge of the upper surface of the reference airfoil. For the smaller stall vortex at  $\alpha = 14^\circ$ , no matter  $\delta_m = 5^\circ$  or  $10^\circ$ , the stall vortex is well controlled. For the larger stall vortex at  $\alpha = 16^\circ$ , the leading edge droop also has a more obvious control effect. As  $\delta_m$  increases, the control effectiveness becomes better.

Fig. 6 shows the comparison of  $C_p$  of the airfoil surface at different leading droop angles and the baseline state when  $\alpha=16^\circ$ . It can be seen that the leading edge droop has the most obvious improvement on the  $C_p$  distribution around  $0.2c-0.3c$  on the upper surface of the airfoil. With the increase of the leading edge droop angle, the  $C_p$  peak value near the leading edge of the upper surface decreases. This is because the relative angle of attack at this position decreases when  $\delta_m$  is large, so  $C_l$  decreases slightly.

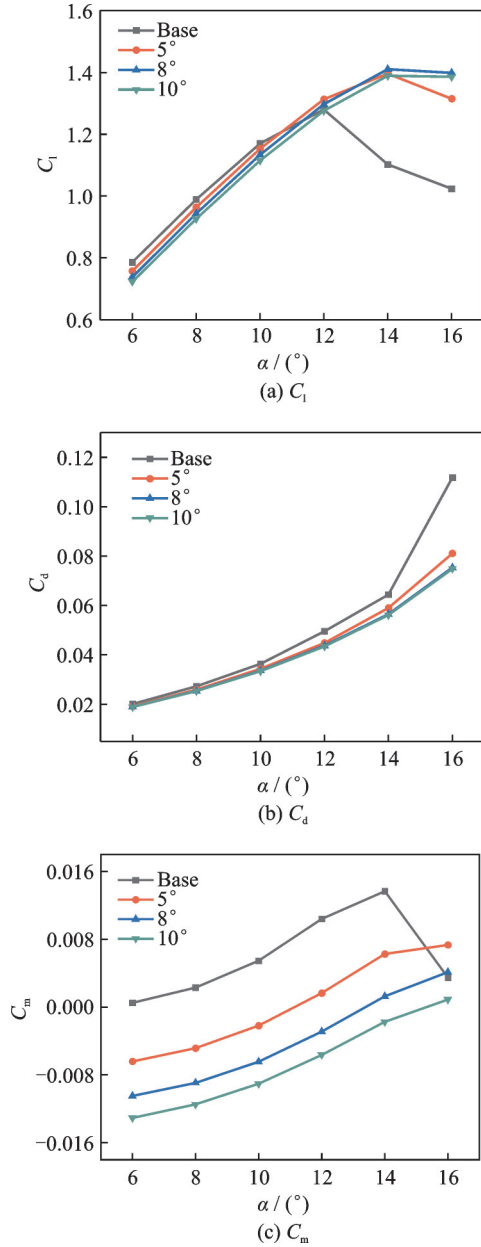


Fig.4 Comparison of aerodynamic characteristics of airfoils

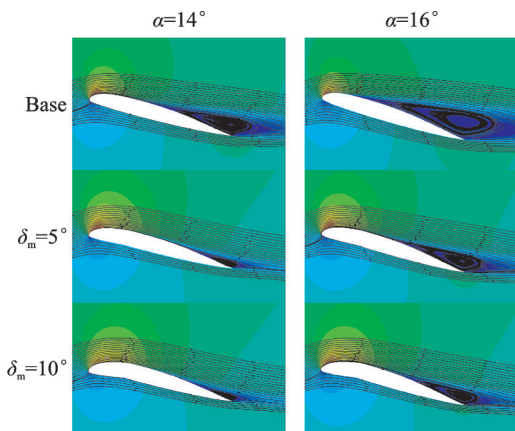


Fig.5 Comparison of airfoil surface flow diagram

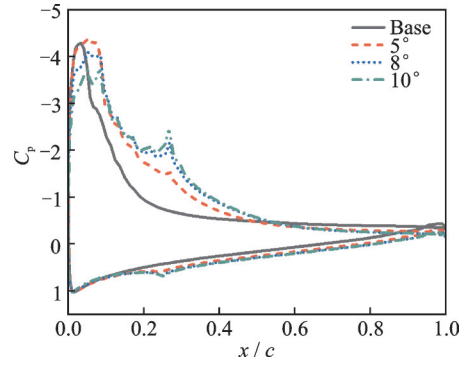


Fig.6 Comparison of airfoil surface pressure coefficient  $C_p$  ( $\alpha=16^{\circ}$ )

### 3 Influence of Leading Edge Droop on Aerodynamic Characteristics of Rotor in Hover State

In this paper, the research on the leading edge droop of 3-D blades is mainly aimed at the modified 7A rotor in order to save the calculation cost. Two blades are selected after modification, and the chord length is 0.2 m. The leading droop position mainly aims at  $r/R=0.75-1$ . The influences of fixed droop angles of  $5^{\circ}$ ,  $8^{\circ}$  and  $10^{\circ}$  on the aerodynamic characteristics of the blade hovering are studied, as shown in Fig.7.  $C_T$  and  $C_Q$  are rotor thrust and torque coefficients, respectively. The larger the leading edge droop angle is, the greater the lift loss will be when  $\theta_0$  is less than  $14^{\circ}$ . This is because the area near the tip of the paddle is an important source of lift. The leading edge droop leads to a decrease in the relative angle of attack of the leading edge and a decrease in lift. For the torque coefficient of the rotor, the torque decreases more obviously with the increase of the leading edge droop angle. However, at a smaller  $\theta_0$ , such as  $6^{\circ}$ , a larger droop angle will cause an increase in the torque coefficient. It can be seen from the hover efficiency  $F_M$  that when  $\delta_m = 8^{\circ}$ ,  $F_M$  increases when  $\theta_0 = 16^{\circ}$  is the maximum. When  $\theta_0$  is greater than  $12^{\circ}$ , the leading edge droop can bring better  $F_M$  promotion effect.

Fig.8 shows the comparison between the baseline state at  $\alpha = 16^{\circ}$  and the equivalent vorticity map near the blade tip calculated by Q-criterion when the leading edge droop  $\delta_m = 10^{\circ}$ . It can be seen that under the datum state, there is a large stall vortex on

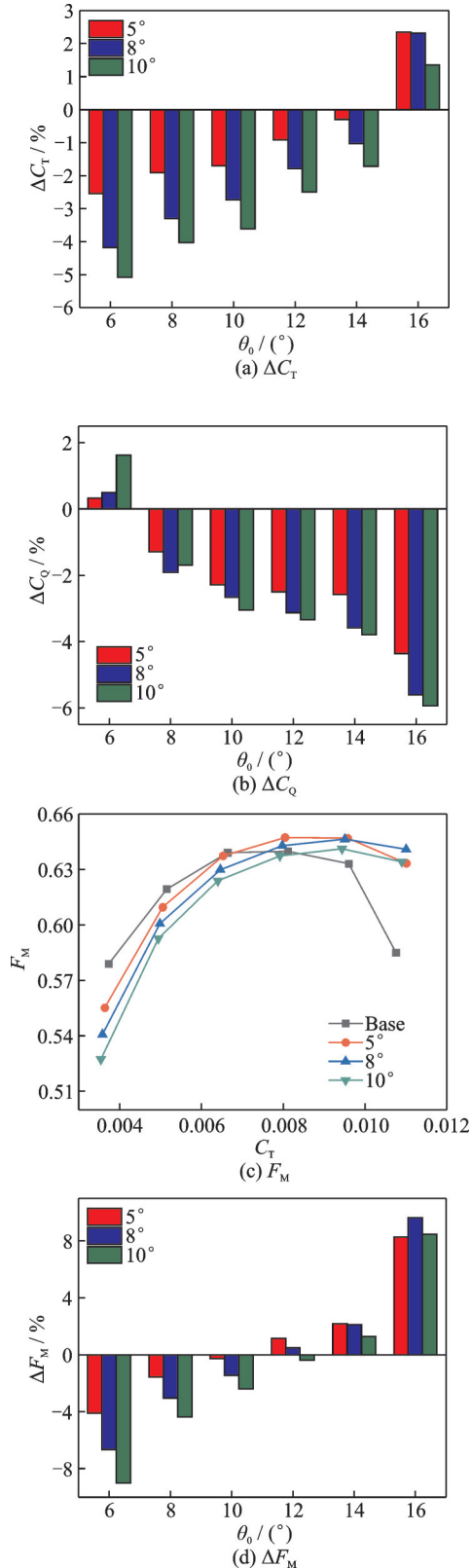


Fig.7 Comparison of aerodynamic characteristics of hovering rotor

the upper surface of the blade tip. Combined with the above analyses, it can be seen that the stall near the blade tip, as the main lift surface, will seriously

affect the aerodynamic characteristics of the blade, and  $F_M$  will be greatly reduced. However, when the leading edge droop  $\delta_m = 10^\circ$  is adopted, there is no obvious stall vortex near the blade tip, and the aerodynamic characteristics are greatly improved.

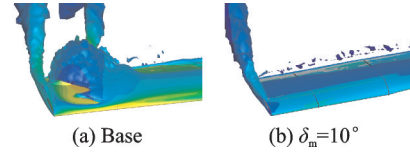


Fig.8 Comparison of equivalent vorticity map near blade tip

Fig.9 shows the comparison of the cloud map of the pressure coefficient on the upper surface of the reference blade at  $\alpha = 16^\circ$  with the leading edge droop  $\delta_m = 10^\circ$ . It can be seen that there is a low pressure area near the leading edge of the blade on the upper surface of the baseline blade, but there is a large high pressure area near the middle chord of the blade tip. This is because there is a large stall vortex and the  $C_p$  caused by airflow separation is small, which has a great impact on the aerodynamic characteristics of hover. After the droop of the leading edge,  $C_p$  is distributed evenly on the upper surface of the blade, and no large  $C_p$  value appears near the leading edge of the blade tip, indicating that there is no airflow separation. Compared with the reference state, the aerodynamic characteristics are greatly improved at this time, indicating that the leading edge sagging can effectively inhibit the generation of stall vortex near the blade tip.

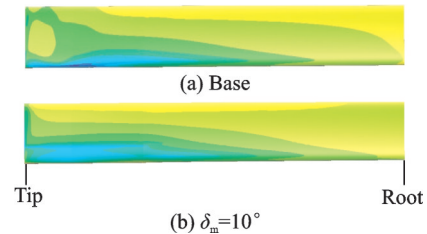


Fig.9 Comparison of pressure coefficient on blade upper surface

## 4 Conclusions

The influences of leading drooping on the aerodynamic characteristics of 2D airfoil and 3D hover

rotor are studied by using the method of motion overset mesh and RBF mesh deformation. From the comparisons of airfoil aerodynamics, rotor hovering efficiency and other parameters, it can be concluded that the leading edge sag can effectively improve the aerodynamic characteristics of 2D airfoil and 3D hovering rotor at high angle of attack, and restrain the generation of stall vortex. For 2D airfoil, the leading edge drooping can effectively delay the stall angle of attack of the airfoil, and has better control effect on the stall vortex on the upper surface of the airfoil near the high angle of attack. It can effectively increase  $C_l$  near the high angle of attack and decrease  $C_d$ , but will cause the overall decrease of  $C_m$ . For rotors in the three-dimensional hovering state, the leading edge droop can only effectively increase the rotor lift near the high angle of attack, but can effectively reduce the torque coefficient at different collective pitch angles and improve the figure of merit near the high collective pitch angle. It has a better control effect on the stall vortex on the upper surface near the blade tip.

## References

- [1] NIU J, LEI J, LU T. Numerical research on the effect of variable droop leading-edge on oscillating NACA 0012 airfoil dynamic stall[J]. *Aerospace Science and Technology*, 2018, 72: 476-485.
- [2] LEE S, MCALISTER K, TUNG C. Characteristics of deformable leading edge for high performance helicopter rotor[C]//*Proceedings of the 11th Applied Aerodynamics Conference*. [S.l.]:AIAA, 1993: 3526.
- [3] KHOSHLAHJEH M, GANDHI F. Extendable chord rotors for helicopter envelope expansion and performance improvement[J]. *Journal of the American Helicopter Society*, 2014, 59(1): 1-10.
- [4] YEO H. Assessment of active controls for rotor performance enhancement[J]. *Journal of the American Helicopter Society*, 2008, 53(2): 152-163.
- [5] EKATERINARIS J A. Numerical investigations of dynamic stall active control for incompressible and compressible flows[J]. *Journal of Aircraft*, 2002, 39(1): 71-78.
- [6] YOU D, MOIN P. Active control of flow separation over an airfoil using synthetic jets[J]. *Journal of Fluids and Structures*, 2008, 24(8): 1349-1357.
- [7] PAPE A L, BEAUMIER P. Numerical optimization of helicopter rotor aerodynamic performance in hover[J]. *Aerospace Science & Technology*, 2005, 9(3): 191-201.
- [8] WANG Q, ZHAO Q. Rotor aerodynamic shape design for improving performance of an unmanned helicopter[J]. *Aerospace Science and Technology*, 2019, 87: 478-487.
- [9] VU N A, LEE J W, SHU J I. Aerodynamic design optimization of helicopter rotor blades including airfoil shape for hover performance[J]. *Chinese Journal of Aeronautics*, 2013, 26(1): 1-8.
- [10] WILKE G. Variable fidelity optimization of required power of rotor blades: Investigation of aerodynamic models and their application[C]//*Proceedings of the 38th European Rotorcraft Forum 2012*. Amsterdam, Netherlands: [s.n.], 2012.
- [11] VU N A, KANG H J, AZAMATOV A I, et al. Aerodynamic design optimization of helicopter rotor blades in hover performance using advanced configuration generation method[C]//*Proceedings of European Rotorcraft Forum*. Germany: [s.n.], 2009.
- [12] CHEN Rongqian, WANG Xu, CHENG Qiyu, et al. Numerical simulation of aerodynamic characteristics of helicopter rotor with tip slots[J]. *Transactions of Nanjing University of Aeronautics & Astronautics*, 2018, 35(6): 942-951.
- [13] JOHNSON C, BARAKOS G. Optimising aspects of rotor blades in forward flight[C]//*Proceedings of the 49th AIAA Aerospace Sciences Meeting Including the New Horizons Forum and Aerospace Exposition*. [S.l.]: AIAA, 2011.
- [14] RENZONI P, D'ALASCIO A, KROLL N, et al. EROS—A common European Euler code for the analysis of the helicopter rotor flowfield[J]. *Progress in Aerospace Sciences*, 2000, 36(5/6): 437-485.

**Acknowledgements** This work was supported by the National Natural Science Foundation of China (No.11972190) and the Aeronautical Science Foundation of China (No. 20185752).

**Authors** Ms. LI Congcong received her M. S. degree in flight vehicle design from Nanjing University of Aeronautics and Astronautics (NUAA) in 2021. Her research interest is focused on rotor aerodynamics and flow control.

Prof. SHI Yongjie received his Ph.D. degree in flight vehicle design from NUAA in 2010. His research interest is focused on rotor aerodynamics, noise control and CFD application.

**Author contributions** Ms. LI Congcong conducted the simulation cases and wrote the manuscript. Prof. SHI Yongjie

designed the study. Prof. XU Guohua and Mr. MA Taihang contributed to the discussion of the study. All authors commented on the manuscript draft and approved the

submission.

**Competing interests** The authors declare no competing interests.

(Production Editor: SUN Jing)

## 基于前缘下垂的提升旋翼悬停气动特性研究

厉聪聪<sup>1,2</sup>, 史勇杰<sup>2</sup>, 徐国华<sup>2</sup>, 马太行<sup>2</sup>

(1. 上海飞机设计研究院, 上海 201210, 中国;

2. 南京航空航天大学直升机旋翼动力学国家级重点实验室, 南京 210016, 中国)

**摘要:** 针对直升机旋翼悬停时, 大拉力附近悬停效率降低的情况, 本文建立了基于前缘下垂的提升旋翼悬停气动特性的数值模拟方法, 以积分形式的雷诺平均 N-S 方程为主控方程。首先以 VR-12 翼型为研究对象, 研究前缘下垂角度对二维翼型气动特性的影响分析。其次, 以修改后的 7A 旋翼为研究对象, 探究了桨叶  $r/R=0.75\sim 1$  位置处不同的前缘下垂角度对悬停状态的气动特性的影响。研究发现, 前缘下垂对大迎角附近的二维翼型及三维悬停旋翼的气动特性均有较为明显的提升, 并且能够有效抑制失速涡的生成。

**关键词:** 直升机旋翼; 悬停; 前缘下垂; 气动特性